Journal of Alloys and Compounds 1065 (2026) 188134

Contents lists available at ScienceDirect

Journal of Alloys and Compounds

journal homepage: www.elsevier.com/locate/jalcom

High-pressure driven anomalous conductions in quasi-one-dimensional Ti_4MnBi_2

Xiao Yao [a,b,1], Guangyang Dai [b,1], Guanghua Liu [b], Zhen Dong [b], Linqian Liu [a,b], Yanru Li [a], Zhihao Wei [a], Xintong Li [a], Yu Liu [b], Xing Wang [b], Fengchun Wei [a,*], Wenhui Liu [b,*], Zheng Deng [c,*], Wenmin Li [b,*], Changqing Jin [c]

[a] School of Materials Science and Engineering, Henan University of Technology, Zhengzhou 450007, China
[b] Institute of Quantum Materials and Physics, Henan Academy of Sciences, Zhengzhou 450046, China
[c] Beijing National Laboratory for Condensed Matter Physics, Institute of Physics, Chinese Academy of Sciences, Beijing 100190, China

ARTICLE INFO

Keywords:
Quasi-one-dimensional chains
Pressure effects
Fermi liquid
Phase transitions
Conductivity

ABSTRACT

Low-dimensional systems serve as ideal platforms for investigating emergent phenomena and dimensional confinement effects in condensed matter physics. Motivated by recent discovered quasi-one-dimensional Ti_4MnBi_2 with possible a quantum critical point, we investigate the evolution of crystal structure and electronic transport properties under pressures. In-situ X-ray diffraction up to 60.3 GPa identify two successive pressure-driven structural transitions at above 9.0 GPa (Phase II) and around 19.5 GPa (Phase III) respectively. Correspondingly, in-situ electrical transport measurements show persistent metallic behavior with increasing conductivity upon compression. Notably, the resistivity temperature exponent, n from the standard fit $R(T) = R_0 + AT^n$, undergoes a distinct change across the two-phase boundaries. The value of n changes from 2 in ambient phase to around 3 in Phase II and return to around 2 in Phase III. The behavior of n close 3 is of particular interest, as it has been observed in correlated systems such as 1*T*-$TiSe_2$ and $Ta_4Pd_3Te_{16}$, which may originate from phonon-assisted interband scattering mechanisms in this compound. The evolution of n across the Phase II and III is reminiscent of dimensional effect, or even a quantum critical scenario.

1. Introduction

In low-dimensional correlated electron systems, dimensional confinement amplifies electronic correlations, quantum fluctuations [1], and anisotropic interactions [2], thereby giving rise to exotic phenomena ranging from spin-charge separation to unconventional superconductivity [3–5]. Especially in one-dimensional (1D) materials, strong quantum fluctuations destroy long-range magnetic order, while electrical transport exhibits pronounced anisotropy [6–8]. Furthermore, instabilities within the 1D bands give rise to a variety of ordered states, such as metal-insulator transitions [9], density wave (DW) order [10], topological phase transitions [11], and unconventional superconductivity (SC) [12–14]. Although ideal 1D materials are difficult to synthesize, quasi-one-dimensional (quasi-1D) systems with well-separated atomic chains serve as a viable platform for exploring characteristic 1D physics. In such systems, weak interchain coupling stabilizes diverse magnetic ground states that can be effectively modulated by pressure [15–19]. The predominantly one-dimensional electronic motion leads to quantum states that are exceptionally sensitive to external perturbations [20–24]. Representative examples include the spin-orbital separation in the 1D Mott insulator Sr_2CuO_3 [25], the dimerized CrS_6 chains with antiparallel spin alignment in ferrotoroidic candidate $Ba_6Cr_2S_{10}$ features [16], and the pressure-induced superconductivity in non-Fermi liquid (FL) Ba_3TiTe_5 [26].

The potential of high-pressure tuning is particularly prominent in Mn-based systems, where the correlation between structural dimensionality and electronic states is subtle and profound [27–29]. For example quasi-1D KMn_6Bi_5 is characterized by infinite $[Mn_6Bi_5]^-$ columnar nanowires containing a Mn-Mn bonded metallic core [30]. High-pressure studies on KMn_6Bi_5 demonstrate that compression-driven modulation of Mn-Mn bond lengths and interchain coupling effectively suppresses magnetic order and induces superconductivity with a

* Corresponding authors.
E-mail addresses: fengchun_wei@haut.edu.cn (F. Wei), whliu@hnas.ac.cn (W. Liu), dengzheng@iphy.ac.cn (Z. Deng), wmli@hnas.ac.cn (W. Li).
[1] These authors contributed equally to this work.

https://doi.org/10.1016/j.jallcom.2026.188134
Received 28 January 2026; Received in revised form 26 March 2026; Accepted 18 April 2026
Available online 20 April 2026

transition temperature (T_c) reaching 9.3 K [31]. These findings reinforce the understanding that in low-dimensional Mn-based intermetallics, pressure-induced structural evolution—particularly the transition of the Mn sub-lattice from 1D chains to a 3D network—serves as the principal mechanism driving pronounced changes in macroscopic electronic and magnetic properties [32].

Recently, Ti_4MnBi_2 with well-separated Mn chains was reported to exhibit features of robust 1D magnetic and electronic properties and furthermore a quantum critical state [33]. However, how this unique chain-like structure and its corresponding transport properties evolve under compression remains an open question. In this work, we present a comprehensive high-pressure study of Ti_4MnBi_2 single crystals, by combining in-situ high-pressure powder X-ray diffraction (XRD) and resistance measurements up to 60.3 GPa. Our study aims to trace pressure-induced structural transitions, identify associated changes in physical properties, and explore the possible emergence of superconductivity. We observe successive structural phase transitions (Phase I → Phase II → Phase III). In Phase II, the resistivity temperature exponent hovers around the value of $n \sim 3.0$. This unusual exponent is commonly attributed to a phonon-assisted *s-d* interband scattering and frequently linked to the onset of superconductivity in correlated electron systems, although it is not a unique signature of superconductivity or criticality. This observation echoes previous studies on Ti_4MnBi_2 which exhibited a quantum critical point at $T = 0$ K via inelastic neutron scattering and theory calculations [33], although there is no direct evidence of whether pressure could extend the quantum critical point in Ref. [33] to higher temperatures. Nevertheless, it still is of great interest to seek new 1D metallic magnets with QCPs that might be accompanied by emergent instabilities such as unconventional superconductivity and electronic delocalization, or new excitations leading to non- FL behavior.

2. Experimental methods

2.1. Sample preparation and characterization

High-quality single crystals of Ti_4MnBi_2 were grown by the self-flux method. High purity starting materials Ti (99.99%), Mn (99.95%), and Bi (99.999%) were mixed at a molar ratio of 4:2:10, placed into an Al_2O_3 tube and sealed inside an evacuated quartz tube. The quartz tube was heated to 1423 K, kept for 30 h, and then cooled to 1073 K at a rate of 3 K/h. At this temperature, the excess Bi-flux was decanted and needle like crystals of typical size 0.5 × 0.5 × 4 mm^3 were obtained. Samples were characterized by X-ray powder diffraction with a Philips X'pert diffractometer using Cu *K*-edge radiation to ensure purity and quality. The temperature dependence of magnetic susceptibility from 2 K to 300 K was measured with a SQUID magnetometer (MPMS3, Quantum Design). The ambient pressure specific heat were performed in a physical property measurement system (PPMS, Quantum Design).

2.2. High-pressure measurements

In-situ high pressure experiments were carried out in a diamond anvil cell (DAC) with a 300 μm in diameter. Cu-Be alloy sheets coated with a c-BN/epoxy mixture were utilized as gaskets and pre-pressed to ~ 45 μm in thickness. A laser-cut hole with a diameter of ~100 μm was created as the sample chamber, and NaCl served as the pressure medium. The temperature-dependent resistivity is measured in a home-made multifunctional measurement system (*Physike*). The pressure was calibrated by using the ruby fluorescence method at room temperature each time before and after the measurement. Synchrotron X-ray diffraction (XRD) measurements at high pressure were conducted at beamline BL15U1 of the Shanghai Synchrotron Radiation Facility (λ = 0.6199 Å). Diamonds with 300 μm culet and rhenium gaskets were used. The pressures were determined by the ruby fluorescence method at room-temperature. The DIOPTAS program was used for integration, and the GSAS II program was employed for refinements on crystal structures under high pressure [34–36].

3. Results and discussion

Ti_4MnBi_2 crystallizes in a V_4SiSb_2-type tetragonal structure with space group *I4/mcm* (No. 140) as shown in Fig. 1(a, b), where Mn atoms arranged into linear chains along the *c* axis, with Mn–Mn distance of 2.49 Å. In the perpendicular *ab* plane, adjacent Mn chains are separated by 7.42 Å, resulting in a highly anisotropic Mn sublattice. Thus, the single crystals grow along the *c*-axis. Each Mn ion is embedded in a square-antiprismatic coordination environment formed by Ti atoms, while Ti and Bi atoms construct extended frameworks surrounding the Mn chains along the chain direction as seen in Fig. 1(c). The inset of Fig. 1(d) shows an optical micrograph of representative single crystals with a needle-like shape and Fig. 1(d) presents the x-ray diffraction patterns perpendicular with the *c*-axis of Ti_4MnBi_2 single crystals. Only a set of (*h k* 0) ($h = k = 1, 2, 3\ldots$) reflections is observed, evidencing a well-defined crystallographic orientation. The narrow diffraction linewidths attest to the high crystalline quality of the samples [37,38]. We performed composition analysis with Energy Dispersive X-Ray Spectroscopy (EDX). Six spots from three single crystals were probed with typical size of 3 × 3 μm. There are negligible divergences among them, indicating the good homogeneity. Given the precision of EDX, the avarice composition $Ti_{3.9}Mn_{1.1}Bi_{2.0}$ is consistent with the nominal Ti:MnBi = 4:1:2. Fig. 1(e) shows the temperature dependence of resistance ($\rho(T)$) along *c*-axis, showing metallic behavior up to 300 K. At low temperature region, a downward is found at around 6 K as indicated by the arrow in the inset of Fig. 4, corresponding to the upturn on the $C_P(T)$ curve. Between 10 and 50 K, $\rho(T)$ is fitted with $\rho(T) = \rho_0 + AT^n$, where ρ_0 is residual resistance, and n for resistivity temperature exponent. The obtained $n \sim 2.0$ indicates the Fermi liquid behavior.

Fig. 2(a) shows the specific heat C_p/T versus T at lower temperature range. The inset presents the specific heat $C_P(T)$ between 2 K and 80 K. $C_p/T(T)$ shows an upward with decreasing temperature at around 6 K, which is consistent with the downward on the $\rho(T)$ curve. With decreasing temperature, a broad maximum peak near 2.4 K appears on $C_p/T(T)$ curve. A similar anomaly was previously reported at 1.9 K from measurements extending down to 0.45 K [39]. The small shift in the peak position may be attributed to the slight difference in compositions. The broad nature of this feature is consistent with frustrated magnetic ordering in Ti_4MnBi_2 reported before [39]. Thus, the $\rho(T)$ downward at 6 K could be attributed the forming of antiferromagnetic (AFM) ordering. It is noteworthy that the transition peaks on specific heat curves are sharp for canonical 3D AFM material. However, the inter-chain two nearest Mn is well separated with distance of 7.42 Å crystal, resulting into a quasi-1D magnetic system. Thus, the inherent magnetic frustration leads to broad and weak AFM transition and exhibits a hump on $C_p/T(T)$.

Fig. 2(b) displays the linear fitting result of C_p/T plotted as a function of T^2 in the temperature range of 10–18 K. The data are well described by

$$C_p/T = \gamma + \beta T^2,$$

where γ is the Sommerfeld coefficient and β characterizes the lattice heat capacity coefficient. The restricted fitting range was chosen to minimize magnetic contributions that become significant below 10 K. The excellent linearity of the fitting curve confirms the validity of this approach. We obtain γ= 57(2) mJ·mol^{-1}·K^{-2} and β= 1.07(0) mJ·mol^{-1}·K^{-4} (Debye temperature, Θ_D = 233.4 K),both consistent with the reported values [39].

Magnetic susceptibility measurements reveal anisotropic AFM order in Ti_4MnBi_2 and its pronounced sensitivity to external magnetic fields. As shown in Fig. 3(a), under a magnetic field of 10 kOe applied parallel to the *c* axis (along the Mn-chain direction), the temperature dependent susceptibility χ_c(T) exhibits a sharp drop at $T_N \approx 2.4$ K, signaling the

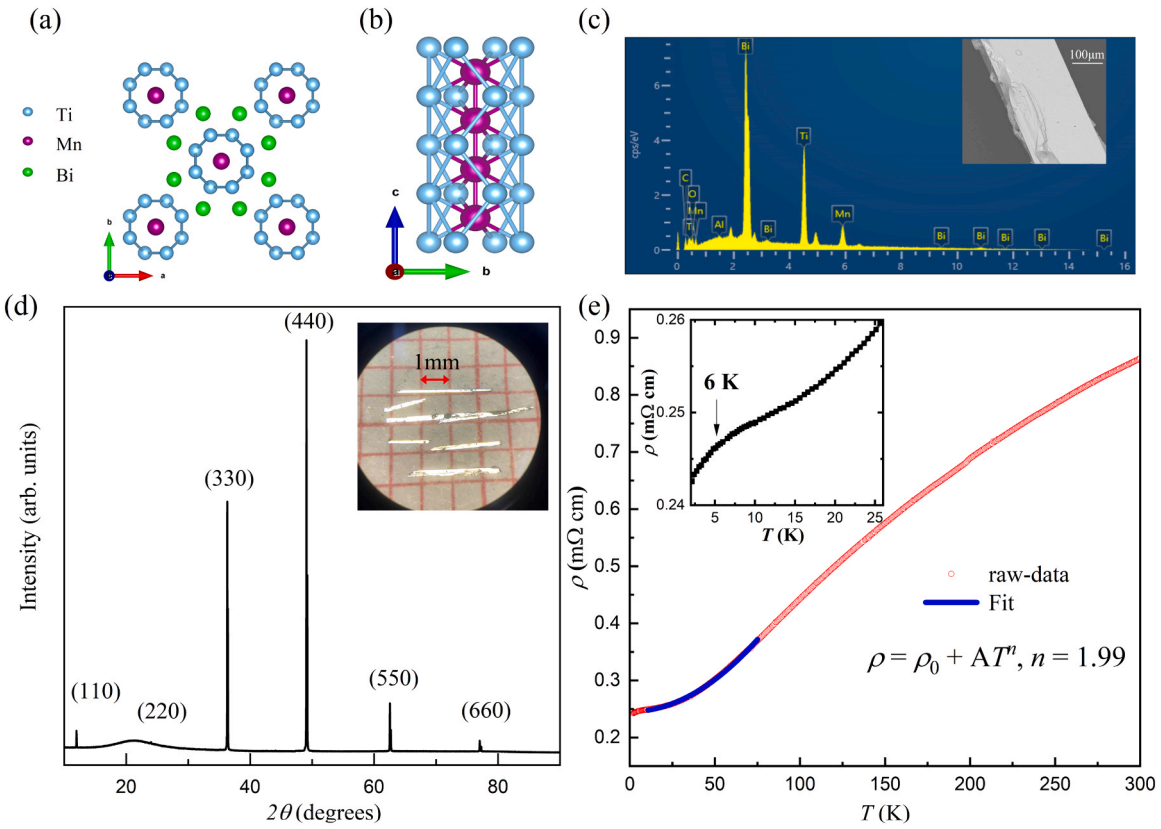

Fig. 1. (a-b) Crystal structure of the tetragonal Ti_4MnBi_2. (c) EDX spectrum of Ti_4MnBi_2 crystals. (d) Single-crystal x-ray diffraction pattern of Ti_4MnBi_2 single crystal. (Inset) A photograph of the Ti_4MnBi_2 crystals on a millimeter-grid paper. (e) Temperature dependence of the resistivity of Ti_4MnBi_2 along the *c*-axis. (Inset) the resistivity-temperature curve at low temperatures shows a kink at $T \sim 6$ K.

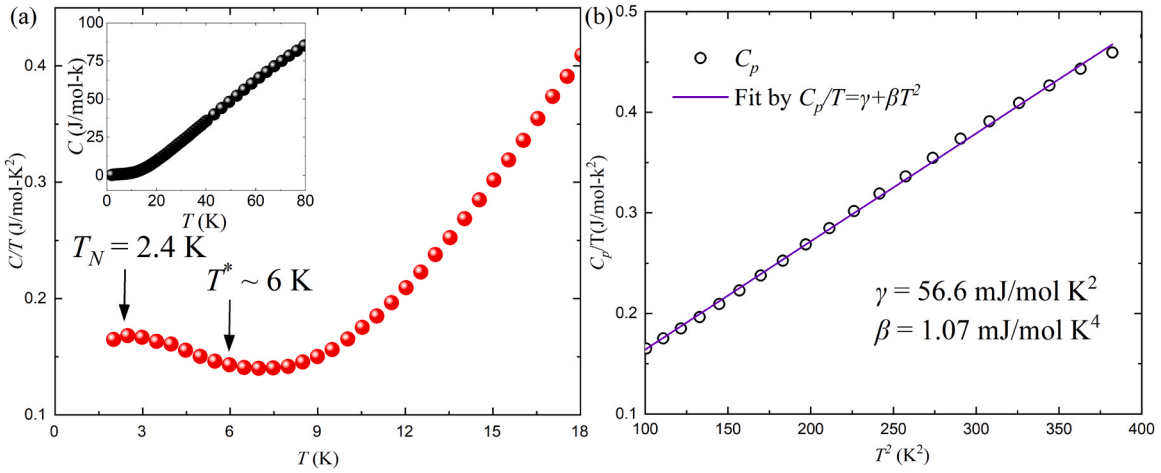

Fig. 2. Temperature dependence of the specific heat of Ti_4MnBi_2. (a) C_p/T versus T at lower temperature range, which show an upward at around 6 K. A broad peak is observed near 2.4 K, potentially associated with antiferromagnetic ordering. The inset presents the specific heat between 2 K and 80 K. (b) $C_P/T(T^2)$ and the corresponding fitting curve for temperatures $100 \leq T^2 \leq 350$, The data points exhibit an excellent linear relationship.

onset of AFM order. This transition temperature is consistent with the anomaly observed in the specific heat [39]. In contrast, when the field is applied perpendicular to the *c*-axis, $\chi_{ab}(T)$ displays only a broadened maximum without a distinct step. This anisotropic response reflects the directional nature of the AFM order, with the transition being more clearly resolved for fields applied along the chain direction. Such behavior is characteristic of low-dimensional antiferromagnets with anisotropic spin correlations. Notable, at around 20 K both $\chi_c(T)$ and $\chi_{ab}(T)$ curves show remarkable divergence for different external fields. This behavior implies presence of short-range magnetic interaction far above T_N. The 2.4 K drop will be gradually suppressed under a magnetic field until it completely disappeared when the applied magnetic field reaches 50 kOe, as shown in Fig. 3(b). The Curie-Weiss fit with data of high-temperature (200 ~ 300 K) yields effective magnetic moment $M_{eff} = 2.65\mu_B$/Mn and Weiss temperature θ = -60.89 K. The large $\theta/T_N = 25.3$ evidences a highly frustrated magnetic ordering. Fig. 3(d-e) shows the field dependent magnetization $M(H)$ at varying temperatures. The $M(H)$ plots are pronounced nonlinear at 20 K that is far from T_N.

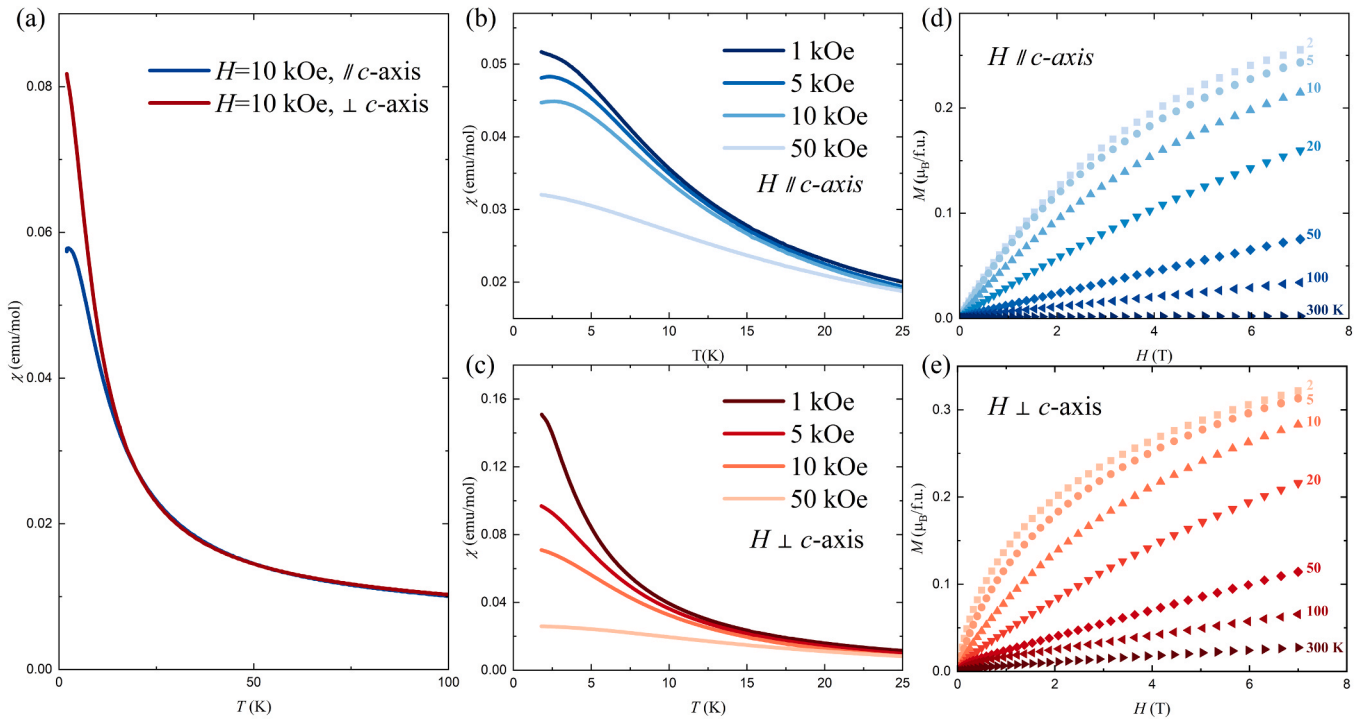

Fig. 3. (a) Temperature dependence of the magnetic susceptibility $\chi = M/H$ of Ti_4MnBi_2. The red data are for a 10 kOe field applied perpendicular to the c-axis, while the green data are for the same field applied along the *c*-axis. (b-c) Temperature dependencies of $\chi_c(T)$ and $\chi_{ab}(T)$ measured at six different fields between 1 and 50 kOe, as indicated. All fields were applied parallel to the *c*-axis. (d-e) Isothermal magnetization $M(H)$ measured with the field $H \| c$-axis and $H \perp c$ at seven different temperatures, as indicated.

This feature is consistent with the divergence on $\chi_c(T)$ curves. The $M(H)$ plots become more nonlinear with decreasing temperature, implying the increased frustration in AFM states. Overall, the observed magnetic behaviors are consistent with the quasi-one-dimensional magnetic state in Ti_4MnBi_2.

To investigate the changes of crystal structure under high pressure and potential correlation with physical properties, high-pressure synchrotron X-ray diffraction measurements were performed on Ti_4MnBi_2 single crystals. Fig. 4(a) presents the X-ray diffraction spectra at various pressures up to 60.3 GPa. In the low-pressure range below 5.7 GPa, the diffraction patterns remain unchanged, indicating that the ambient-pressure tetragonal phase (Phase I) is stable in this regime. With increasing pressure to 9.0 GPa, additional diffraction peaks emerge in the 12–13° range and gradually higher with further compression, manifesting the occurrence of a structural phase transition to a first high-pressure phase (Phase II). It is worth noting that the diffraction pattern remains unchanged up to 5.7 GPa, indicating that the structural transition initiates somewhere within the pressure of 5.7 ~ 9.0 GPa, and the phase coexistence near the boundary is highly common [23]. At higher pressures around 19.5 GPa, some of the diffraction peaks Phase II disappear, hinting at a transition to another high-pressure phase (Phase III). As pressure increases to the highest measured value of 60.3 GPa, the diffraction peaks of both the ambient-pressure phase and the high-pressure phase gradually weaken but do not vanish completely. Although a complete structural refinement of the high-pressure phases remains unavailable, we tried to perform indexing of the high-pressure XRD spectra (shown in Fig. S1) using the least-squares method. The results revealed the presence of two tetragonal phases after structural transformations. Phase III was well-fitted by the model, whereas certain peaks in Phase II could not be reasonably accounted for. This discrepancy is likely attributable to phase coexistence rather than an abrupt phase transition in this pressure region. We try to fit the lattice parameters and the interchain distances between the two nearest Mn ions as shown in Fig. S2. As the pressure increases, the lattice parameters decrease monotonically, exhibiting nearly isotropic behavior, with a slightly higher compression rate along the *c* direction. A weak discontinuity could be observed at the phase boundary, indicating the occurrence of the phase transition. The detailed analysis can be found in the Supplementary Materials. Notably, throughout the entire pressure range investigated, the diffraction peaks remain sharp and well defined, with no evidence of peak broadening or amorphization. This confirms that Ti_4MnBi_2 preserves long-range crystalline order up to at least 60.3 GPa. We also collected Raman spectra up to 59.4 GPa as displayed in Fig. 4 (b), (c) and Fig. S3. At low pressure, the A_{1g} mode near 240 cm^{-1} exhibits a distinct splitting, which gradually merges into a single peak above ~3.9 GPa, implying the presence of slightly inequivalent local bonding environments that are suppressed upon further compression. In contrast, the low-frequency B_{2g} mode around 70 cm^{-1} shows pronounced anomalies and eventually disappears with increasing pressure, reflecting symmetry breaking within the *ab*-plane. Meanwhile, the A_{1g} mode persists throughout the entire pressure range and continuously shifts to higher frequencies, indicative of bond stiffening along the quasi-1D chain direction. The transition pressures inferred from Raman spectroscopy are lower than those detected by XRD, highlighting the higher sensitivity of Raman scattering to subtle local distortions. Taken together, these results demonstrate that the *I4/mcm* structure undergoes a pressure-induced lattice distortion with reduced symmetry, preceded by local symmetry breaking and fully reversible upon decompression.

High-pressure X-ray diffraction reveals a sequence of two pressure-induced structural transformations in Ti_4MnBi_2 at around 9 GPa and 19.5 GPa, respectively. In the following section, we examine how these pressure-driven structural evolutions affect the electronic transport properties. Electrical transport measurements of Ti_4MnBi_2 single crystals were performed up to 53.4 GPa. As shown in Fig. 5, the resistance decreases monotonously under compression, consistently exhibited metallic behavior across the entire pressure range. At around 7.6 GPa, the *R–T* curves show a pronounced abrupt drop, with the overall resistance decreasing by nearly one order of magnitude. Based on the XRD

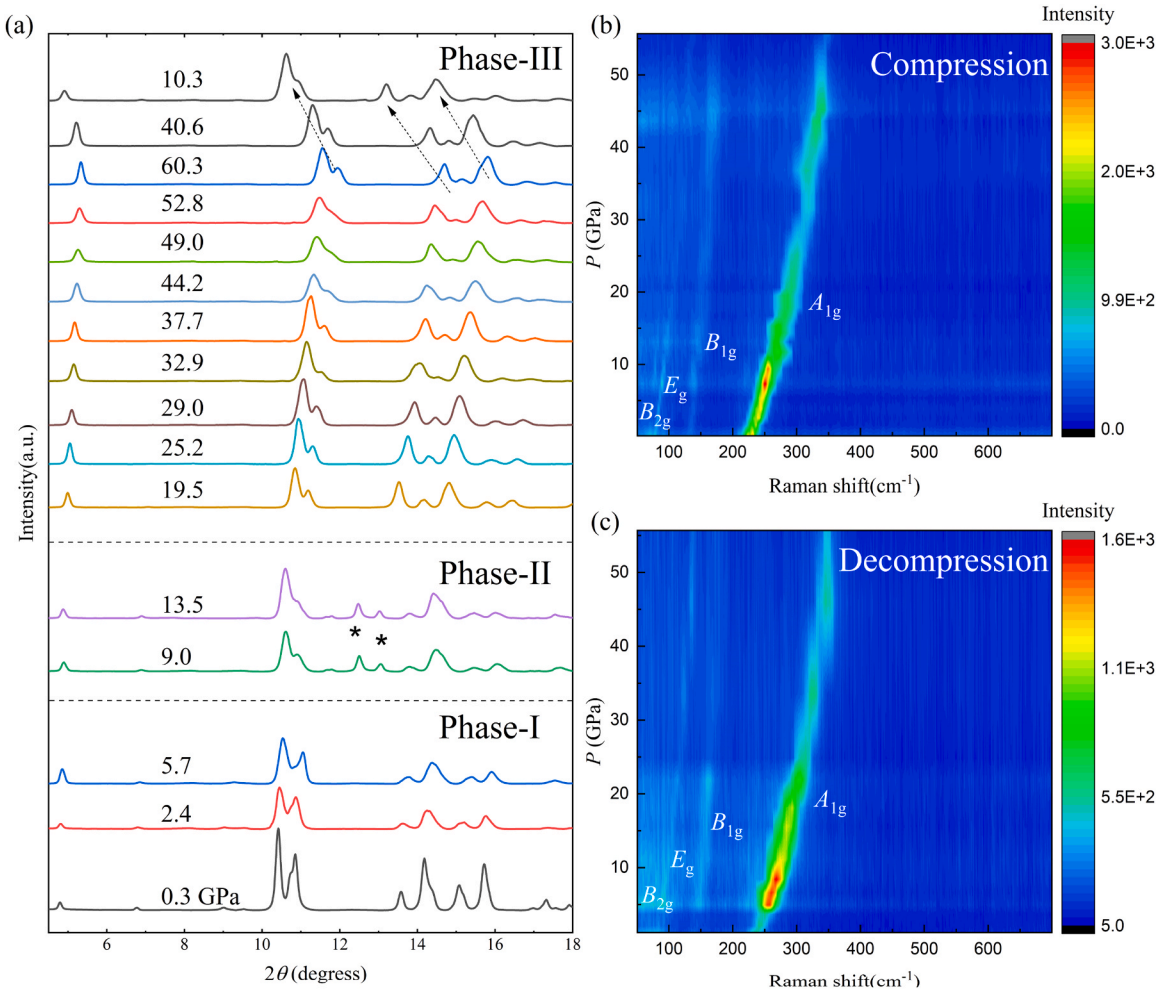

Fig. 4. (a) High-pressure synchrotron x-ray diffraction patterns of Ti_4MnBi_2 powder collected under various pressures at room temperature (λ = 0.6199 Å). The asterisks mark the new diffraction peaks belonging to the high-pressure phase at 9.0 GPa. 2D plots of Raman spectra up to 55.7 GPa at room temperature, with (b) Compression and (c) Decompression.

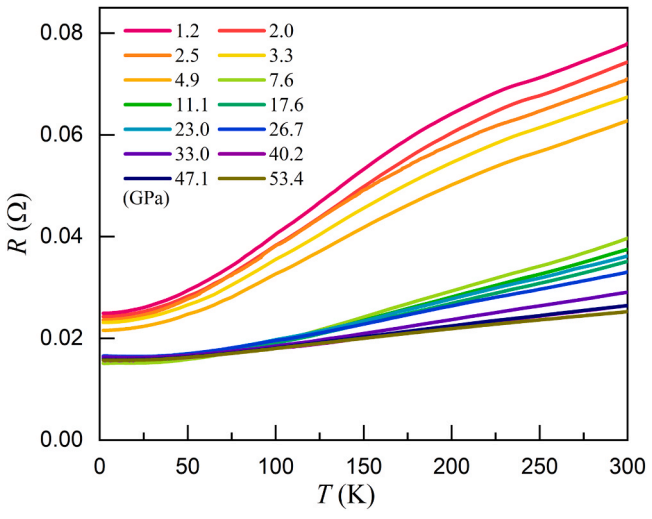

Fig. 5. Pressure evolution of resistance-temperature curves in Ti_4MnBi_2 single crystal.

results, the phase transition from Phase I to Phase II occurs within the 5.7 ~ 9.0 GPa range. The slight difference in the observed transition pressure between transport and diffraction measurements can be attributed to several factors inherent to high-pressure experiments. The two sets of measurements were performed in separate diamond anvil cell setups, which may involve minor differences in pressure medium, or hydrostatic conditions. Transport properties—being highly sensitive to the formation of a percolative conductive path—can detect the emergence of a new phase at a lower volume fraction, whereas XRD requires a substantial volume fraction for the new peaks to be observable. Therefore, the resistance drop at ~7.6 GPa is consistent with the onset of the pressure-induced structural phase transition and marks the point at which the electronic response becomes sensitive to the structural change. The enhanced charge transport of the high-pressure phase suggests a significant reconstruction of the electronic band structure, likely arising from either a sharp increase in carrier concentration due to band overlap or from reduced carrier scattering as quasi-1D chain fluctuations are suppressed in the high-pressure phase.

No signal of superconductivity was observed. The absent of superconductivity could be the consequence of incomplete suppression of the antiferromagnetism within the pressure and temperature ranges of our measurements. It is noteworthy that in both 1*T*-$TiSe_2$ and $Ta_4Pd_3Te_{16}$, the appearance of superconductivity is accompanied by suppression of a magnetic order to a quantum critical point. For 1*T*-$TiSe_2$, superconductivity emerges only after the charge density wave (CDW) order is suppressed, forming a dome-shaped superconducting phase diagram [40]. Recent studies have revealed that the superconducting state in 1*T*-$TiSe_2$ is closely linked to a pressure-induced Lifshitz transition and

Fermi surface reconstruction, leading to a two-gap superconducting state with enhanced superfluid density [41]. In $Ta_4Pd_3Te_{16}$, superconductivity appears at $T_c \approx 4.6$ K at ambient pressure, and pressure tuning further optimizes T_c up to ~ 6.5 K, with a well-defined superconducting dome and anomalous normal-state transport properties [42]. On closer examination, we study the evolution of the resistivity temperature exponent under the increasing pressures as shown in Fig. 6. Each value of n was obtained through a fitting procedure over the low temperature region of up to 50 K (Fig. S4). For Phase I, the resistivity exponent hovers around the value of $n = 2$, indicating a normal FL behavior. Upon increasing pressure to 7.6 GPa, where a structural transition is inferred, n shows a dramatic increase to 2.7. Within Phase II n retains around 3 regardless of a steady decrease. This unusual exponent is clearly different from $n = 2$ for electron-electron (FL) or $n = 5$ for electron-phonon scattering, respectively. The behavior of $n = 3$ is commonly attributed to a phonon-assisted *s-d* interband scattering. The similar behavior is observed in 1*T*-$TiSe_2$ and $Ta_4Pd_3Te_{16}$, where superconductivities were tightly correlated with the unusual resistivity exponent [40,42]. It is worth noting that many of the 1D systems show Luttinger liquid behavior which also show resistivity exponent deviating from $n = 2$ [43]. Thus the possibility of the Luttinger liquid behavior for Phase-II, as well as the trivial pressure-induced change between FL and Luttinger liquid behavior, could not be ruled out in this work. In Phase III, the exponent is completely suppressed to $n = 2$. It should be noted that the extracted exponent n is obtained over the temperature range of 10 ~ 50 K. Considering the Debye temperature $\Theta_D \approx 233$ K derived from specific heat measurements, phonon contributions to resistivity may already become non-negligible within this fitting window. Therefore, the fitted n values should be regarded as effective exponents, reflecting contributions from multiple scattering channels including both electron–electron and electron–phonon interactions. Overall, the systematic evolution of n across the structural transitions—from ~2 in Phase I to ~3 in Phase II and back to ~2 in Phase III—clearly indicates a pressure-induced crossover in the dominant scattering regime. This behavior highlights the strong sensitivity of electronic transport properties to structural modifications in this quasi-one-dimensional system. The feature may be originated from dimensional effect, or even reminiscent of a quantum critical scenario. The effective quasiparticle mass and specific heat under high pressure would indeed provide crucial supporting evidence, which is also what we will intend to explore.

4. Conclusions

In summary, we systematically investigate the pressure effects on crystal structures and electronic conduction of quasi-1D Ti_4MnBi_2 single crystals up to 60.3 GPa. External pressure drives two successive structural phase transitions (Phase I → Phase II → Phase III), accompanied by a continuous enhancement of electronic conductivity. A distinct resistance drop coincides with the emergence of Phase II. Remarkably Phase II shows a clear deviation from standard Fermi-liquid behavior, with $n \approx 3$, while Phase I and Phase III exhibit Fermi-liquid behavior with a resistivity temperature exponent $n \approx 2$. Intriguingly, the similar exponents have been reported in unconventional superconductors 1*T*-$TiSe_2$ and $Ta_4Pd_3Te_{16}$, although it is not a unique signature of superconductivity or criticality. Moreover, the systematic suppression of n back to 2 near the Phase II–III boundary reflects the sensitivity of the electronic scattering mechanisms to pressure-driven structural changes. Further experiments for the effective quasiparticle mass and specific heat under high pressure would be valuable to explore the possible quantum critical point and more dimensional effects. This work establishes a direct connection between pressure-driven structural evolutions and correlated physical properties in Ti_4MnBi_2, and provides valuable insights into the dimensionality engineering of quasi-1D systems via external pressure.

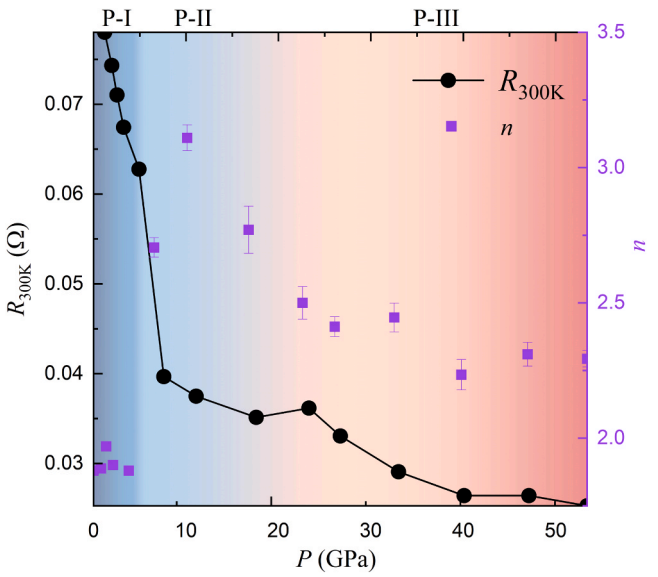

Fig. 6. The phase diagram of quasi-1D Ti_4MnBi_2 as a function of pressure up to 60 GPa. The resistances ($R_{300\,K}$) and the resistivity temperature exponent n versus the pressures for Ti_4MnBi_2. P-I, P-II and P-III stand for Phase-I, Phase-II and Phase-III, respectively.

CRediT authorship contribution statement

Linqian Liu: Investigation. **Yanru Li:** Investigation. **Changqing Jin:** Writing – review & editing, Conceptualization. **Guanghua Liu:** Investigation, Formal analysis. **Zhen Dong:** Investigation. **Wenhui Liu:** Writing – review & editing, Writing – original draft, Methodology, Investigation, Formal analysis. **Xiao Yao:** Investigation, Formal analysis, Data curation. **Zheng Deng:** Writing – review & editing, Visualization, Formal analysis, Data curation, Conceptualization. **Guangyang Dai:** Investigation, Formal analysis, Data curation. **Fengchun Wei:** Writing – review & editing, Writing – original draft, Supervision, Methodology, Data curation. **Wenmin Li:** Writing – review & editing, Visualization, Supervision, Data curation, Conceptualization. **Yu Liu:** Formal analysis. **Xing Wang:** Formal analysis. **Zhihao Wei:** Investigation. **Xintong Li:** Investigation.

Declaration of Competing Interest

The authors declare that they have no known competing financial interests or personal relationships that could have appeared to influence the work reported in this paper.

Acknowledgments

This work is supported by the National Natural Science Foundation of China (Grant No. 12404008), and the High-level Talent Research Start-up Project Funding of Henan Academy of Sciences (Project No. 241827046, 242027151, 241827011), the Fundamental Research Fund of Henan Academy of Sciences (Project No. 240627005, 20250627007), the Natural Science Foundation of Henan (Project No. 242300420640), the CAS Project for Young Scientists in Basic Research (No. YSBR-030), the Open Research Fund for Beijing National Laboratory for Condensed Matter Physics (Project No. 2023BNLCMPKF006), the Henan Provincial Science and Technology Research Project (Project No. 252102230027), the College Student Innovation Training Program (Project No. 202510463025), the Postgraduate Innovation Project of Henan Academy of Sciences (Project No. 243327003) and the Innovation Program for Quantum Science and Technology (Grant No. 2021ZD0302800). We thank the Shanghai Synchrotron Radiation Facility of Experiment Assist

System (https://cstr.cn/31124.02.SSRF.LAB) for the assistance on pressure calibration.

Appendix A. Supporting information

Supplementary data associated with this article can be found in the online version at doi:10.1016/j.jallcom.2026.188134.

References

[1] A.M. Tsvelik, O.M. Yevtushenko, Quantum phase transition and protected ideal transport in a Kondo chain, Phys. Rev. Lett. 115 (2015) 216402.

[2] L. Liu, Y. Pan, M. Cheng, N. Zhou, X. Zhu, R. Zhang, W. Song, C. Xi, G. Li, X. Luo, Y. Sun, Anisotropic magnetoresistance and quantum oscillations in a quasi-one-dimensional topological semimetal Ta_2PdSe_6 single crystal, Phys. Rev. B 113 (2026) 035118.

[3] L. Duan, J. Zhang, X. Wang, Z. Zhao, C. Xiao, X. Li, Z. Hu, J. Zhao, W. Li, L. Cao, G. Dai, C. Ren, X. He, R. Yu, Q. Liu, L.H. Tjeng, H.-J. Lin, C.-T. Chen, C. Jin, High pressure phase of Ba_2FeS_3: An antiferromagnet with one-dimensional spin chains, J. Alloy. Compd. 859 (2021) 157839.

[4] W.H. Liu, X.L. Yi, W.C. Li, X.Z. Xing, H.J. Zhao, M.X. Xu, Z.X. Shi, Transport properties and phase diagrams of $FeSe_{1-x}S_x$ ($0 \leq x \leq 1$) single crystals, J. Alloy. Compd. 919 (2022) 165760.

[5] K. Wang, Q. Hou, Y.Q. Shi, S.N. Zhang, Z.Y. Liang, W.H. Liu, X. Zhou, W. Wei, Z. A. Ren, S. Li, Z.X. Shi, Superconductivity of $La_3Ni_2O_{7-\delta}$ ($-0.09 \leq \delta \leq 0.3$) with different oxygen stoichiometry under high pressure, J. Alloy. Compd. 1061 (2026) 187448.

[6] Y.-Y. Wang, Z.-K. Yi, N. Li, Y.-R. Li, P. Su, Y. Zhou, D.-D. Wu, Y. Sun, Q.-J. Li, X.-Y. Yue, X. Zhao, X.-F. Sun, H. Liang, Magnetic and electrical transport properties of quasi-one-dimensional Ln_3HfBi_5 single crystals (Ln = Pr, Nd, Sm), Phys. Rev. B 110 (2024) 134432.

[7] W.-H. Jiao, Y. Liu, P. Tao, J. Lu, X. Liang, W. Yang, Z. Zhang, S. Xu, Y. Luo, Z.-W. Zhu, D. Qian, X. Xu, Z. Ren, G.-H. Cao, S. Xiao, Large magnetoresistance and quantum oscillations in quasi-one-dimensional ternary telluride $TaCo_2Te_2$, Phys. Rev. B 111 (2025) 045109.

[8] Z. Wang, G. Wang, W. Li, Z. Wang, R. Chen, L. Duan, J. Zhao, Z. Deng, J. Zhang, T. Yan, J. Zhang, X. Wang, C. Jin, High-pressure synthesis and structure of quasi-one-dimensional Ba_3MSe_5 (M = Ti, Zr, and Hf), Inorg. Chem. 64 (2025) 13705–13714.

[9] D. Jerome, C. Bourbonnais, Quasi one-dimensional organic conductors: from Fröhlich conductivity and Peierls insulating state to magnetically-mediated superconductivity, a retrospective, Comptes Rendus. Phys. 25 (2024) 17–178.

[10] M. Moromizato, T. Miyake, T. Masuda, T. Kimura, K. Kimura, Imaging and control of magnetic domains in a quasi-one-dimensional quantum antiferromagnet $BaCu_2Si_2O_7$, Phys. Rev. Lett. 133 (2024) 086701.

[11] L. Yang, D. Wang, Z. Hu, Z. Dong, Y. Zhang, K. Tang, P. Wang, J. Zhang, C. Chen, X. Hou, J. Li, Q. Yu, J. Wang, L. Wang, K. Zhang, Quasi-one-dimensional Ta_2PdSe_6 with strong topological surface states for high-performance and polarization-sensitive terahertz detection, Nano Lett. 25 (2025) 7690–7698.

[12] Y.L. Huang, Z.Y. Zhang, Z.Y. Liu, P.T. Yang, B. Li, C.Q. Xu, B.S. Wang, W. Zhou, W.-H. Jiao, S. Xu, Z. Zhu, T. Shiroka, X. Xing, Za Xu, D. Qian, S. Li, X. Ke, J.G. Cheng, X. Xu, Transport and quantum oscillations in the quasi-one-dimensional superconductor V_2Ga_5, Phys. Rev. B 111 (2025) 024503.

[13] R. Sun, H. Li, D. Zhang, D. Meng, C. Zhao, S. Jin, Gene-inherited [Se_2] dimers in a reactive salt flux: synthesis of a quasi-one-dimensional $NbSe_2$ superconductor, J. Am. Chem. Soc. 147 (2025) 24201–24205.

[14] J. Wang, L. Hu, S. Li, C. Jiang, Z. Li, Q. Tao, F. Qu, L. Lu, G. Liu, Z.-A. Xu, Superconductivity in the quasi-one-dimensional ternary compound $Ca_3Pt_4Bi_8$, Phys. Rev. B 110 (2024) 144520.

[15] G.-Y. Dai, X. He, Z.-W. Li, C.-L. Zhang, L.-C. Shi, R.-Z. Yu, X.-C. Wang, C.-Q. Jin, Physical properties and phase diagram of $NaFe_{1-x}V_xAs$, Chin. Phys. B 30 (2021) 017401.

[16] J. Zhang, X. Wang, L. Zhou, G. Liu, D.T. Adroja, I. da Silva, F. Demmel, D. Khalyavin, J. Sannigrahi, H.S. Nair, L. Duan, J. Zhao, Z. Deng, R. Yu, X. Shen, R. Yu, H. Zhao, J. Zhao, Y. Long, Z. Hu, H.-J. Lin, T.-S. Chan, C.-T. Chen, W. Wu, C. Jin, A ferrotoroidic candidate with well-separated spin chains, Adv. Mater. 34 (2022) 2106728.

[17] X. Zheng, J. Tan, Q. Wang, C. Gao, X. Yu, W. Xie, Y. Yang, Y. Wang, C. Jin, Pressure-induced first-order antiferromagnetic to ferromagnetic transition in MnN, J. Alloy. Compd. 935 (2023) 168120.

[18] J. Zhang, Y. Jia, X. Chen, B. Min, T. Honda, Z. Hu, L.H. Tjeng, S.-i Shamoto, J. Zhao, Z. Deng, J. Song, L. Duan, M. Valvidares, J. Zhu, X. Wang, C. Jin, Structure and properties of $Ba_9Fe_3S_{15}$ with quasi-one-dimensional spin chains, Phys. Rev. B 111 (2025) 224405.

[19] W.H. Liu, J.J. Feng, W. Zhou, S. Li, Z.X. Shi, High-pressure studies on quasi-one-dimensional systems, Chin. Phys. B 34 (2025) 088104.

[20] L. Duan, X. Wang, J. Zhang, J. Zhao, Z. Zhao, C. Xiao, C. Guan, S. Wang, L. Shi, J. Zhu, C. Jin, Critical behavior of the ferromagnetic metal La_3CrAs_5 with quasi-one-dimensional spin chains, J. Alloy. Compd. 905 (2022) 164214.

[21] S. Xu, Z. Liu, P. Yang, B. Ruan, Z. Ren, J. Sun, Y. Uwatoko, B. Wang, J. Cheng, From semiconductor to Fermi metal and emergent density-wave-like transition in the quasi-one-dimensional n-type $Bi_{19}S_{27}I_3$ under hydrostatic pressure, Phys. Rev. B 109 (2024) 144107.

[22] Y. Zhang, H. Zhao, J. Li, R. Dai, Z. Wang, Z. Wang, Z. Zhang, High-pressure superconducting phases in quasi-one-dimensional $(TaSe_4)_3I$, Phys. Rev. B 112 (2025) 064515.

[23] W.H. Liu, J.J. Feng, Q. Hou, B. Li, K. Wang, B. Chen, S. Li, Z.X. Shi, Pressure-induced superconductivity and isosymmetric structural transition in quasi-one dimensional Ta_2PdS_6, Phys. Rev. B 109 (2024) 054513.

[24] F. Ke, S. Niu, J. Feng, K. Yin, M. Han, H. Yang, B.Y. Wang, A. Celeste, C. Jia, B. Chen, L. Wang, H.Y. Hwang, Y. Tian, W.L. Mao, Y. Lin, Superconductivity in compressed quasi-one-dimensional face-sharing hexagonal perovskite chalcogenides, Sci. Adv. 11 (2025) eadv1894.

[25] J. Schlappa, K. Wohlfeld, K. Zhou, M. Mourigal, M. Haverkort, V. Strocov, L. Hozoi, C. Monney, S. Nishimoto, S. Singh, A. Revcolevschi, J.S. Caux, L. Patthey, H. Ronnow, J. van den Brink, T. Schmitt, Spin–orbital separation in the quasi-one-dimensional Mott insulator Sr_2CuO_3, Nature 485 (2012) 82–85.

[26] J. Zhang, Y. Jia, X. Wang, Z. Li, L. Duan, W. Li, J. Zhao, L. Cao, G. Dai, Z. Deng, S. Zhang, S. Feng, R. Yu, Q. Liu, J. Hu, J. Zhu, C. Jin, A new quasi-one-dimensional compound Ba_3TiTe_5 and superconductivity induced by pressure, NPG Asia Mater. 11 (2019) 60.

[27] Y. Deng, Y. Yu, M.Z. Shi, Z. Guo, Z. Xu, J. Wang, X.H. Chen, Y. Zhang, Quantum anomalous Hall effect in intrinsic magnetic topological insulator $MnBi_2Te_4$, Science 367 (2020) 895–900.

[28] Y. Zhou, L. Chen, L. Zhao, S. Long, Y. Wang, X. Qiu, C. Chai, Z. Guo, Q. Zhang, J. Guo, K. Liu, Q. Lin, L. Sun, J. Hu, G. Wang, Progress in quasi-one-dimensional Mn-based superconductors, Sci. Sin. Phys. Mech. Astron 53 (2023) 127413.

[29] S. Huyan, T. Qian, L. Wang, W. Bi, F. Xue, D. Zhang, C. Hu, B. Kalkan, Y. Huang, Z. Li, A. Das, J. Schmidt, R.A. Ribeiro, T.J. Slade, N. Ni, P.C. Canfield, S.L. Bud'ko, Pressure-induced changes in structure, magnetic order and development of superconductivity in the ferromagnetic topological insulator $MnBi_8Te_{13}$, arXiv 2512 (2025) 15667.

[30] J.-K. Bao, Z.-T. Tang, H.J. Jung, J.-Y. Liu, Y. Liu, L. Li, Y.-K. Li, Z.-A. Xu, C.-M. Feng, H. Chen, D.Y. Chung, V.P. Dravid, G.-H. Cao, M.G. Kanatzidis, Unique $[Mn_6Bi_5]^-$ nanowires in KMn_6Bi_5: a quasi-one-dimensional antiferromagnetic metal, J. Am. Chem. Soc. 140 (2018) 4391–4400.

[31] P.-T. Yang, Q.-X. Dong, P.-F. Shan, Z.-Y. Liu, J.-P. Sun, Z.-L. Dun, Y. Uwatoko, G.-F. Chen, B.-S. Wang, J.-G. Cheng, Emergence of superconductivity on the border of antiferromagnetic order in $RbMn_6Bi_5$ under high pressure: a new family of Mn-based superconductors, Chin. Phys. Lett. 39 (2022) 067401.

[32] C. An, Y. Zhou, C. Chen, F. Fei, F. Song, C. Park, J. Zhou, H.G. Rubahn, V. V. Moshchalkov, X. Chen, G. Zhang, Z. Yang, Long-range ordered amorphous atomic chains as building blocks of a superconducting quasi-one-dimensional crystal, Adv. Mater. 32 (2020) 2002352.

[33] X.Y. Li, A. Nocera, K. Foyevtsova, G.A. Sawatzky, M. Oudah, N. Murai, M. Kofu, M. Matsuura, H. Tamatsukuri, M.C. Aronson, Frustrated S=1/2 chains in one-dimensional correlated metal, Nat. Mater. 24 (2025) 716–721.

[34] J. Zhang, Y. Jia, X. Chen, B. Min, T. Honda, Z. Hu, L.H. Tjeng, S.-i Shamoto, J. Zhao, Z. Deng, J. Song, L. Duan, D. Valvidares, J. Zhu, X. Wang, C. Jin, Structure and properties of $Ba_9Fe_3S_{15}$ with quasi-one-dimensional spin chains, Phys. Rev. B 111 (2025) 224405.

[35] X. He, C.L. Zhang, Z.W. Li, K. Lu, S.J. Zhang, B.S. Min, J. Zhang, L.C. Shi, S. M. Feng, Q.Q. Liu, J. Song, X.C. Wang, Y. Peng, L.H. Wang, V.B. Prakapenka, S. Chariton, H.Z. Liu, C.Q. Jin, Superconductivity discovered in niobium polyhydride at high pressures, Mater. Today Phys. 40 (2024) 101298.

[36] Q. Liu, X. Yu, X. Wang, Z. Deng, Y. Lv, J. Zhu, S. Zhang, H. Liu, W. Yang, L. Wang, H. Mao, G. Shen, Z. Lu, Y. Ren, Z. Chen, Z. Lin, Y. Zhao, C. Jin, Pressure-induced isostructural phase transition and correlation of FeAs coordination with the superconducting properties of 111-type $Na_{1-x}FeAs$, J. Am. Chem. Soc. 133 (2011) 7892–7896.

[37] C.G. Richter, W. Jeitschko, B. Künnen, M.H. Gerdes, The ternary titanium transition metal bismuthides Ti_4TBi_2 with T= Cr, Mn, Fe, Co, and Ni, J. Solid State Chem. 133 (1997) 400–406.

[38] R. Rytz, R. Hoffmann, Chemical bonding in the ternary transition metal bismuthides Ti_4TBi_2 with T= Cr, Mn, Fe, Co, and Ni, Inorg. Chem. 38 (1999) 1609–1617.

[39] A. Pandey, P. Miao, M. Klemm, H. He, H. Wang, X. Qian, J.W. Lynn, M.C. Aronson, Correlations and incipient antiferromagnetic order within the linear Mn chains of metallic Ti_4MnBi_2, Phys. Rev. B 102 (2020) 014406.

[40] A.F. Kusmartseva, B. Sipos, H. Berger, L. Forró, E. Tutiš, Pressure induced superconductivity in pristine1T-$TiSe_2$, Phys. Rev. Lett. 103 (2009) 236401.

[41] F. Elson, J. Philippe, G. Simutis, O.K. Forslund, M. Abdel-Hafiez, M. Janoschek, R. Khasanov, D. Das, J. Weissenrieder, D.W. Tam, Y. Sassa, M. Månsson, Lifshitz-enhanced superfluid density in two-gap superconducting $TiSe_2$, npj Quantum Mater. 11 (2025) 4.

[42] J. Pan, W.H. Jiao, X.C. Hong, Z. Zhang, L.P. He, P.L. Cai, J. Zhang, G.H. Cao, S. Y. Li, Nodal superconductivity and superconducting dome in the layered superconductor $Ta_4Pd_3Te_{16}$, Phys. Rev. B 92 (2015), 180505(R).

[43] J. Hager, R. Matzdorf, J. He, R. Jin, D. Mandrus, M.A. Cazalilla, E.W. Plummer, Non-fermi-liquid behavior in quasi-one-dimensional $Li_{0.9}Mo_6O_{17}$, Phys. Rev. Lett. 95 (2005) 186402.